

USE OF VECTOR ISOMETRIC ROTATIONS IN THE MEASUREMENT OF IMPERFECTLY ALIGNED ANTENNAS

Stuart F. Gregson, Michael J. Carey
Nearfield Systems Inc.
19730 Magellan Drive,
Torrance, CA 90502-1104

ABSTRACT

Most traditional antenna measurement techniques presume that the antenna under test (AUT) is accurately aligned to the mechanical axes of the test range. Sometimes, however, it is not possible to achieve such a careful antenna alignment [1]. In these cases, standard post processing techniques can be used to accurately correct antenna-to-range misalignment. Alternatively, similar results may be obtained by approximation in the form of piecewise polynomial interpolation. When carefully employed, this method will result in only a small increase in uncertainty, but with a significant reduction in computational effort.

This paper describes this far-field alignment correction method, which is closely related to standard active alignment correction methods [2]. This paper then proceeds to use numerical simulation as well as actual range measurements to demonstrate the effectiveness of this method. Finally, the utility of this technique in the presentation of far-field antenna pattern functions is illustrated.

Keywords: Antenna Alignment, Near-Field Antenna Measurements, Vector Rotation, Genetic Algorithm.

1. Introduction

Generally, the purpose of a range measurement is to characterize the radiation pattern of an AUT at a very great, or infinite, distance with reference to an angular or other co-ordinate set. In principle, the AUT should be accurately aligned to the primary axes of the range. However, in practice, there might be considerable difficulties with achieving such an accurate alignment. These difficulties may be caused by the size or mass of the test antenna, or perhaps by a limitation in the mechanical mounting that might result in a large, cumbersome, or expensive structure. Fortunately, the relationship between the frame of reference associated with the antenna, and that of the range can usually be acquired. Providing this is the case, any misalignment can be corrected for within the data processing chain and a number of techniques exist that can be harnessed for this purpose [1,4]. These techniques generally use modal expansion, which is rigorous for the case of a band-

limited spectrum function, and the necessary processing is intensive [2, 4].

Another approach (the purpose of this paper) is to consider using approximation in a generalised vector isometric rotation strategy that uses two-dimensional interpolation [3]. Often, the use of approximation when implementing alignment corrections has been avoided due to concerns of slightly degraded accuracy. Typically, it has only been used in cases where the alignment data was known and rigorous equivalents were unavailable (*c.f.* cylindrical near-field measurements), where accuracy requirements were not paramount, or during the visualisation of measurements that were known to have an antenna-to-range misalignment.

The latter case primarily involves optimizing the agreement attained between respective measurements by simply varying the amount of rotation being applied to one or the other pattern prior to plotting. Normally, this would be accomplished manually. However, since vector isometric rotations can be implemented efficiently through the use of approximation, it is appropriate for inclusion within the optimisation loop of a genetic algorithm. Thus, this would enable pattern comparisons to be made even in cases where antenna-to-range alignment information was known only approximately, or perhaps even completely absent.

The following sections aim to describe the alignment correction technique, verify its application through numerical simulation and actual range measurements, before concluding with an illustration of its utility within an alignment optimising genetic algorithm.

2. Overview of Antenna Pattern Rotation

Transformation matrices are matrices that multiply a point vector to produce a new point vector. A series of transformation matrices may be concatenated into a single matrix through matrix multiplication. A transformation matrix may represent each of the operations of translation, scaling, and rotation. However, if $[A]$ is a three by three orthogonal, normalised, square, matrix it may be used to specify an isometric rotation that can be used to relate two frames of reference, *i.e.* two co-ordinate systems. We may write that a point in one frame of reference can be

specified in terms of a point in the other frame of reference using,

$$\begin{bmatrix} u' \\ v' \\ w' \end{bmatrix} = [A] \cdot \begin{bmatrix} u \\ v \\ w \end{bmatrix} \quad (1)$$

Here primed co-ordinates are used to differentiate between the respective systems. However, if the rotation is assumed to comprise an x -, y -, and z -rotation where the rotations have been applied in that order, then $[A]$ can be obtained from,

$$[A] = \begin{bmatrix} 1 & 0 & 0 \\ 0 & c(x) & s(x) \\ 0 & -s(x) & c(x) \end{bmatrix} \cdot \begin{bmatrix} c(y) & 0 & -s(y) \\ 0 & 1 & 0 \\ s(y) & 0 & c(y) \end{bmatrix} \cdot \begin{bmatrix} c(z) & s(z) & 0 \\ -s(z) & c(z) & 0 \\ 0 & 0 & 1 \end{bmatrix} \quad (2)$$

Here, c and s denote the trigonometric functions cosine and sine respectively. Crucially, although almost any number of different angular definitions are available for describing the relationship between the respective co-ordinate systems, they can be related, *i.e.* equated, to one another via the direction cosine matrix. In the case of applying a scalar (no polarization change) rotation to an antenna pattern, the algorithm would be as follows:

1. Calculate the equivalent triad of Cartesian direction cosines (u, v, w) corresponding to each of the points in the pattern, *i.e.* directions in the raster grid of sampling nodes which is usually a grid of spherical angles *e.g.* a plaid, monotonic and equally spaced grid of $-\text{say} - \theta$ and ϕ angles.
2. Transform the triad of direction cosines, using equations (1) and, for example, (2) to compute the equivalent direction cosines in the other rotated frame of reference (u', v', w').
3. Calculate the equivalent spherical angles in the second rotated co-ordinate system. Note: this will generally represent an irregular non-rectilinear co-ordinate system.
4. Approximate the new rotated pattern function from the original data set using which ever interpolating scheme is best suited to the underlying pattern function, *e.g.* bi-linear, bi-cubic, *etc.*.
5. Plot new data using regular raster grid of spherical angles.

This generic process can be used to rotate an antenna pattern that has been tabulated in any of the conventional far-field plotting co-ordinate systems, *e.g.* azimuth over elevation, elevation over azimuth, polar spherical, true-view, direction cosine, *etc.* [5]. Clearly, this can be repeated for each polarisation component.

In contrast, a vector rotation (as required to implement an alignment correction to an antenna measurement) changes both the pattern and polarisation. Unfortunately, the by-

product of a scalar rotation is that the reference, *i.e.* observing, polarisation is rotated with the pattern by exactly the same amount as the pattern has been rotated – after all we did nothing to the polarisation, we merely rotated the pattern so it had no alternative but to be rotated with the pattern. Thus, an inverse rotation must be applied to the polarisation basis in order that the observing polarisation can be returned to its original state. Fortunately, this can be accomplished simply by utilizing the inverse of equation (1) to correct the field components. In summary, the algorithm for applying a vector rotation to an antenna pattern can thus be expressed as follows:

1. Resolve the far-field pattern (*e.g.* initially resolved onto a Ludwig III polarisation basis) onto a Cartesian polarisation basis.
2. Apply a scalar rotation to each of the three polarisation patterns (separately) using the algorithm detailed above.
3. Apply an inverse isometric rotation to the interpolated field components to complete the vector isometric rotation.
4. Resolve the far-field pattern back onto the desired polarisation basis (*e.g.* Ludwig III definition).

3. Preliminary Simulated Results

In order to verify the post-processing technique described above, simulated far-field patterns were obtained where a radiator was aligned to the axes of the simulation space, and where it was rotated with respect to the simulation space. The purpose of this was to test the vector isometric rotation by taking the rotated data set and computing the nominally aligned data set that could then be compared with the nominally aligned reference set. To this end, a proprietary three dimensional, full wave computational electromagnetic (CEM) solver employing the finite difference time-domain (FDTD) method was used to solve for the electric and magnetic fields. In this case, a simple open-ended rectangular waveguide (OEWG) section, excited by the fundamental TE_{10} mode was modelled twice, once when the axes of the OEWG were aligned with the axes of the simulation space, and again with the OEWG section having been rotated through 30° about the x -axis of the space. This can be seen illustrated schematically in Figure 1.

The choice of an elementary OEWG section was made as this was both simple to model and the low gain nature of the device enables pattern comparisons to be made over very nearly the complete far-field sphere.

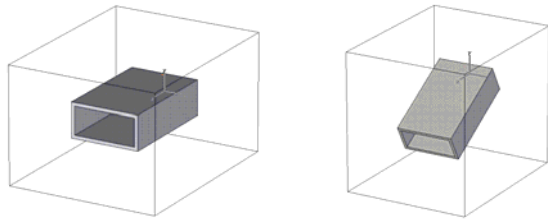


Figure 1 – Nominally aligned waveguide section (left) & rotated waveguide section (right).

The Cartesian components of the far-field patterns of these simulations can be seen presented in Figure 2, Figure 3, and Figure 4 plotted using a regular azimuth over elevation co-ordinate system over the complete far-field sphere. These have been plotted together with the alignment corrected patterns where the agreement can be seen to be very encouraging for each of the triad of Cartesian field components. Although not shown, the agreement between the resulting phase patterns was equally encouraging with only very minor differences being evident which result from the slightly different phase origins that were used in the respective CEM simulations.

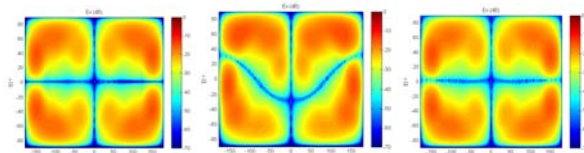


Figure 2 – Nominally aligned OEWG (left), rotated OEWG (centre), re-aligned OEWG (right).

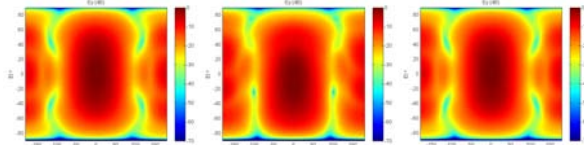


Figure 3 – Nominally aligned OEWG (left), rotated OEWG (centre), re-aligned OEWG (right).

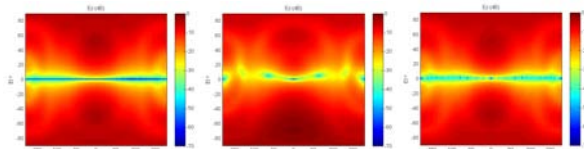


Figure 4 – Nominally aligned OEWG (left), rotated OEWG (centre), re-aligned OEWG (right).

4. Preliminary Measured Results

The acquisition of the crucial antenna-to-range alignment data will vary from facility to facility. Within a spherical system an optical alignment method is often employed [6]. Conversely, a planar facility may utilise a procedure

that involves touching-off contact points on the antenna using a precision mechanical contacting probe [6]. Unfortunately, in some cases, it is either not possible to acquire this information or it is not obtained with sufficient accuracy to be of very great use. In instances such as these when in all other respects the measurements are sound, and it is merely the alignment that is questionable, it would be useful to be able to deduce the “idealised” alignment and plot the patterns taking into account all the changes in the pointing and polarisation of the pattern.

Motivated by the requirement to demonstrate the validity of the alignment correction with spherical near-field antenna measurements (very encouraging results have previously been obtained for the case of planar near-field measurements [2, 6]), a simple genetic algorithm was developed which attempted to breed the optimum alignment information so that an imperfectly aligned antenna could be plotted as though the measurements had been taken with nominally idealised antenna-to-range alignment. Figure 5 shows the NSI-700S-80 over-head scanning-arm spherical near-field measurement system together with the pyramidal horn antenna that was used as the AUT. This antenna was selected as it is mechanically rigid, *i.e.* gravitationally insensitive, and had a low gain. The latter property equates to radiating significant field intensities at wide out angles that enables pattern comparisons to be performed over a larger portion of the forward half-space.



Figure 5 – NSI-700S-80 Spherical near-field system testing X-band pyramidal horn.

The near-field data was acquired and transformed to the far-field tabulated on a regular azimuth over elevation coordinate system and resolved onto a Ludwig III copolar and cross-polar polarisation basis and can be seen presented in Figure 6.

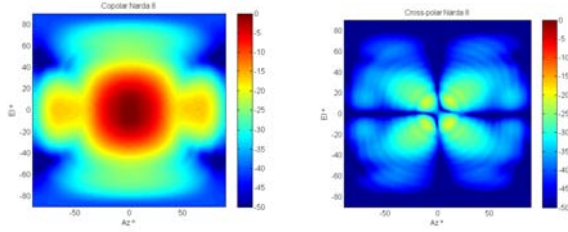


Figure 6 – Copolar (left) & cross-polar (right) far-field pattern of nominally aligned pyramidal horn.

Some range multipath can be seen in these plots and is most likely a result of the close proximity of the electrically, comparatively, thin absorber which was used to cover certain parts of the system during this preliminary measurement campaign. The pyramidal horn was removed from this system and a then reinstalled with an additional mounting bracket installed between the range (lower ϕ axis) positioner and the AUT. This consisted to two aluminium wedges which were bolted together at 90° degrees as shown in Figure 7, which were intended to introduce a deliberate mispointing to the antenna-to-range alignment. The near-field pattern of the horn was acquired and transformed to the far-field.

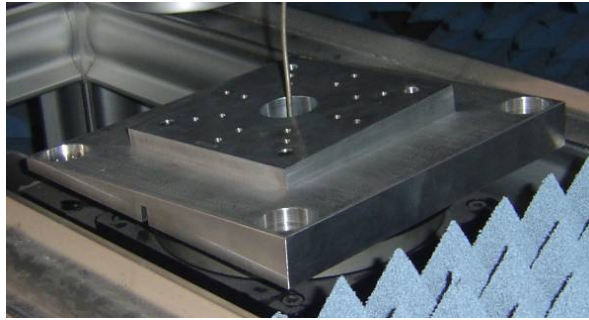


Figure 7 – Alignment shims used to introduce a known AUT pointing.

Here, the angle between the back and front face of the larger wedge was 5.14° and 2.38° for the smaller wedge. Using equation (2) the equivalent direction cosine matrix can be calculated thus allowing the alignment correction to be implemented. In order that the proposed genetic optimiser could be verified, the alignment matrix was initialised as being the identity matrix. Then, a series of small random rotations were applied and the resulting pattern compared with the reference set. If the agreement improved, as determined by evaluating the SSD, this was deemed to be a successful generation and these rotations were kept. Clearly, if the resulting patterns were in

poorer agreement than its parents were, the previous set of rotations were retained as the basis for another generation. This procedure can be found illustrated schematically in Figure 8.

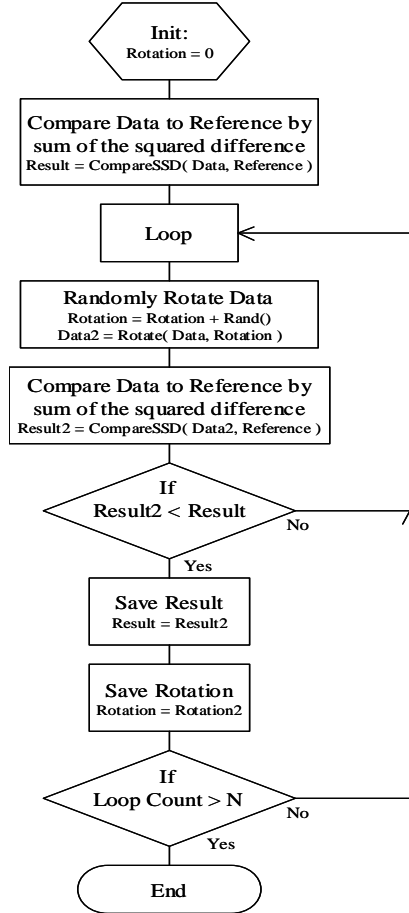


Figure 8 – Schematic of alignment recovery algorithm.

The sum-squared difference (SSD) between the respective far-field patterns was used as an error metric or penalty function (*c.f.* iterative near-field phase retrieval algorithms) within the genetic algorithm. This is computed by summing the squared difference of the calculated modulus of the two pattern sets, *i.e.* $|u_{i,j}|$, and $|v_{i,j}|$, at each point (i,j) over the copolar *and* cross-polar patterns. Mathematically, this can be expressed as follows,

$$\xi_{SSD} = \frac{\sum_{i,j} (|u(i,j)| - |v(i,j)|)^2}{\sum_{i,j} |v(i,j)|^2} \quad (3)$$

There is nothing special about using the SSD between the patterns as a penalty function and many other measures of adjacency are available and could have been used instead, *e.g.* cross-correlation coefficient or ordinal measure of adjacency [2]. However, the SSD has the benefit of being comparatively computationally inexpensive and has

proved to be relatively robust, yielding a useful measure of convergence. As an example, a plot of the SSD for each successful generation can be seen in Figure 9.

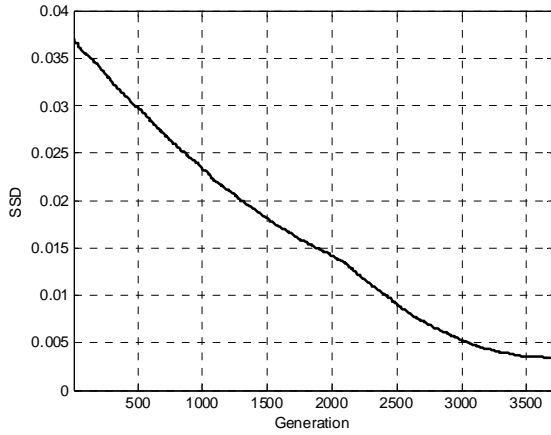


Figure 9 – Plot of SSD showing convergence of genetic optimisation algorithm.

Here, it can be seen that the iterative algorithm appears to have converged after breeding approximately 3500 successful generations – only approximately one in four generations were deemed to represent a benefit over their antecedence. When the algorithm was terminated, the value of the pair of angles was 4.9053° and 2.261° . Figure 10 contains the copolar and cross-polar far-field alignment corrected pattern obtained when this optimised alignment correction is used.

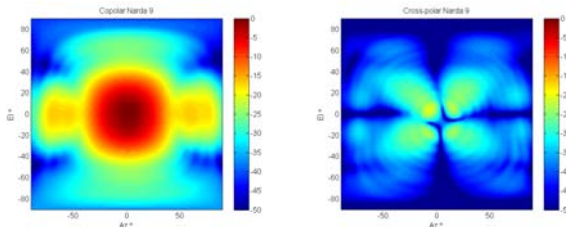


Figure 10 – Copolar (left) & cross-polar (right) far-field pattern of alignment corrected pyramidal horn.

From inspection of Figure 6 and Figure 10, it is apparent that the agreement attained is encouraging, although some differences, mainly at wide angles and in the cross-polar pattern are evident. Figure 11 contains an isolevel, *i.e.* contour, plot of the three far-field patterns. Here, dotted contours are used to denote the nominally aligned pattern measurement, continuous black contours denote alignment corrected pattern using measured angles, and continuous grey contours are used to denote alignment corrected pattern data where the alignment angles were deduced using the genetic optimiser. Here, the difference between the black and grey contours results from the differences in the alignment information used to correct these patterns. Clearly, although the measured and

reconstructed angular amounts differ from one another, their impact on the ensuing corrected far-field patterns is comparatively minor and probably sufficiently good for the intended purpose of pattern comparison.

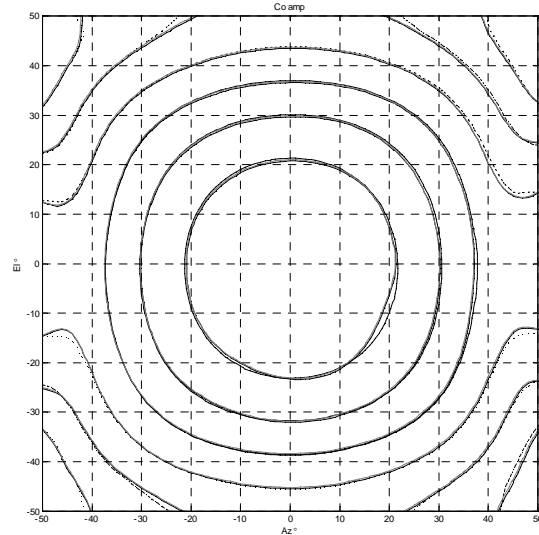


Figure 11 – Comparison of boresight region of far-field copolar patterns.

Interestingly, the sum-squared difference between the nominally aligned pattern and the alignment corrected pattern where the angular values were taken from measurements of the wedges was $\xi_{SSD} = 0.0035$, conversely when using the rotations obtained from the genetic algorithm $\xi_{SSD} = 0.0034$ and from inspection, it could be seen that the contours were, subjectively, in better alignment. Despite some care being taken in the alignment of the “nominally” aligned measurement, it is possible that this measurement contained some slight imperfection in its alignment that would potentially explain this slight difference and which was borne out by the fact that the peak of the pattern was not precisely on boresight (the low gain, broad beam pattern of the AUT can make exact determination of the peak of the pattern challenging as, for example, it can easily be disturbed by spurious noise on in the measurement, *e.g.* range multiple reflections, *etc.*). This multi-path also degraded the agreement attained at wide out pattern angles where signal levels are lower and gain slopes smaller.

5. Summary and Conclusion

The successful use of a genetic algorithm in recovering antenna-to-range alignment has been demonstrated. It is important to recognise that this algorithm optimises the alignment of one measurement to another and yields patterns that are in “best” agreement, as determined by a measure of similarity, *i.e.* adjacency. However, if the

reference measurement set contains an imperfection in its alignment, then the recovered antenna-to-range alignment will also contain this same error within the determined values.

Clearly, approximate methods such as those deployed herein can prove unreliable on occasion. For example, the results may become inaccurate if used to correct very high gain antenna patterns where the underlying pattern function fluctuates rapidly with respect to the sampling interval. Errors may also be encountered in regions of low signal levels where the presence of noise can disturb the interpolation, *e.g.* in pattern nulls. Interpolation formulas tend to use several neighbouring points (sampling nodes) to approximate an interleaving point. Thus, although being suppressed localised noise will be “spread out” to any interpolated point using a noise contaminated sampling node. However, for many cases where the rotation has been accomplished using approximation, rather than rigorous sampling theorem (*i.e.* Whittaker) interpolation, the results are usually sufficiently reliable for the purposes of visualisation, which indeed is the intent here.

In conclusion, this paper has shown that a simple vector isometric rotation, employing an efficient polar implementation of a bi-cubic convolution interpolation algorithm, can be used to obtain reliable alignment corrected results that are in very close agreement with those results obtained by more intensive, rigorous means. Although it is always possible to choose a function that is sufficiently pathological to make a mockery of any interpolating procedure, in practice this implementation has been found to be comparatively robust. Although the subject of ongoing research requiring further verification, a new alignment optimisation algorithm has been presented that enables relative alignment information to be deduced between pairs of far-field antenna patterns.

6. REFERENCES

- [1] S.F. Gregson, J. McCormick, “The Application of Non-Rectilinear Co-Ordinate Systems In The Characterisation Of Mis-Aligned Space Antennas”, AMTA 1999.
- [2] S.F. Gregson, J. McCormick, C.G. Parini, “Principles of Planar Near-Field Antenna Measurements”, IET Electromagnetic Waves series 53, 978-0-86341-736-8, 2007.
- [3] R.G. Keys, “Cubic Convolution Interpolation for Digital Image Processing”, IEEE Trans. on Acoustics, Speech, and Signal Processing, Vol. 29, No. 6, Dec. 1981, pp. 1153-1160.
- [4] A. Frandsen, “Spherical Near-Field Transformation Program With Probe Correction”, TICRA, Denmark, 1995.
- [5] G.F. Masters, S.F. Gregson, “Co-ordinate System Plotting For Antenna Measurements”, AMTA St-Louis, 2007.
- [6] S.F. Gregson, A.J. Robinson, “An Inter-range Comparison in Support of the Characterisation of Space Antenna Systems and Payload Testing”, IEE, 1998.

ACKNOWLEDGEMENTS

The authors wish to extend their gratitude to John Demas, Greg Hindman, Bert Schluper, Dan Slater, and Bruce Williams, for their many valuable comments, suggestions and encouragement on this effort.